Journal of Sound and Vibration (2000) **233**(1), 41–61
doi:10.1006/jsvi.1999.2789, available online at http://www.idealibrary.com on IDEAL®

SPANWISE COUPLING OF CELLULAR STRUCTURES IN 2-D AND TAPERED CIRCULAR CYLINDER WAKE UNDER ACOUSTIC EXCITATION

F.-B. Hsiao and C.-H. Chiang

Institute of Aeronautics and Astronautics, National Cheng Kung University, Tainan, Taiwan, Republic of China

(*Received* 12 *September* 1997, *and in final form* 13 *November* 1999)

The wake behind a two-dimensional (2-D) and tapered circular cylinder was locally excited by acoustic waves to invesigate the spanwise coupling of cellular shedding vortices by means of hot-wire measurements. The experiments were conducted in a low-speed wind tunnel, with the operating Reynolds number based on the mean diameter fixed at $1{\cdot}0 \times 10^4$. The cellular structure of the shedding vortices in the wake behind a 2-D circular cylinder can be enhanced and locked in to the artificial perturbations. Three lock-in regions with different ratios of the response frequency to the excitation frequency were identified. As for the wake behind the tapered cylinder, the cellular distribution of the natural shedding frequency was significantly restored when the acoustic waves were introduced at a reasonable level of excitation. In addition, the length of the spanwise lock-in region extending leftward and rightward from the exciting slot would reach a saturated value and the saturated lock-in remains almost the same for the three slot locations tested.

1. INTRODUCTION

The cellular structure of shedding vortices in the wake flow behind a tapered circular cylinder is a special phenomenon of flow instability, which was first studied by Gaster [1, 2] in the laminar wake and lately by Hsiao *et al.* [3] in the turbulent wake. An intriguing characteristic of cellular structures in this kind of flow is the stepwise distribution of shedding frequencies in the wake. In fact, the stepwise distribution of the shedding frequencies also takes place in the wake behind a constant-diameter (2-D) cylinder due to the influence of the end effect [4, 5], the non-uniform oncoming flow [6], and the diameter discontinuity of the model [7, 8].

An important research topic with regard to the cellular distribution of the shedding frequencies is the formation mechanism of cells in the wake. Gaster [1] and Noack *et al.* [9] had separately proposed mathematical analogue models to explain the formation of cells. The main concept they proposed was to take the spanwise coupling into consideration in the governing equations in which the wake was regarded as a dynamic system composed of numerous subsystems in some kinds of oscillators with different original oscillating frequencies while coupled with each other. Their results demonstrated that this dynamic system exhibited the cellular behavior of the shedding vortices. Though the concept of the spanwise coupling can explain the formation of cells, the subsequent question follows as to what generates the coupling mechanism.

Hsiao and Chiang [10] proposed a cell-formation mechanism to explain the generation, propagation and interaction of the instability waves in the spanwise direction of a turbulent

0022-460X/00/210041 + 21 $35.00/0

wake behind a tapered circular cylinder. The experimental results of the vortex lock-in phenomenon by Griffin and Hall [11] provided some evidence to support Hsiao and Chiang's [10] idea of the interaction between the instability waves. If additional disturbances were added inside the absolutely unstable region in the wake behind a 2-D circular cylinder, such as to vibrate the cylinder or to introduce the artificial velocity fluctuations, the state of instability may change depending upon the type and intensity of the additional disturbances. The shedding frequency will deviate from its natural value if the additional disturbances grow to a certain extent to take over the originally most unstable waves. The required intensity of disturbances to lock-in the natural shedding vortices is usually small when the disturbance frequency is close to the natural shedding frequency of the wake. In practice, the so-called response vortex-shedding frequency is intimately related to the forcing intensity, frequency, and position of the excitation introduced. This has been demonstrated by Griffin and Hall's findings [6, 11] about the vortex lock-in phenomeon in which the vortex-shedding frequency behind a bluff body can be modified by the artificial periodic excitation at different frequencies. Williamson [12] also studied the vortex dislocations for the transition of a wake in the natural and forced formation. He found an interesting feature of vortex dislocations having intrinsically rapid spreading in the spanwise direction under the small-ring excitation.

The present study is therefore devoted to an examination of the spanwise coupling of the cellular structures by introducing the acoustic perturbations into the wake behind a 2-D and a tapered circular cylinder respectively. This is relevant to the study of vortex lock-in phenomenon by Griffin [6] and Hsiao *et al.* [3]. However, the artificial perturbations used here will only be emitted through a narrow slot that occupies a small portion of the model, which is in striking contrast to the full-span excitation in our previous study [3]. Therefore, the major purpose in the present study is to investigate the effects of the added acoustic perturbations on the shedding-frequency distribution and the cellular structure coupling in the spanwise direction. As long as the instability waves in the wake behind the tapered cylinder could propagate along the span to influence the shedding vortices at other spanwise locations, the artificially added perturbations should effectively exhibit the same behavior. That is, the lock-in region may not be restricted only in the portion around the slot position; instead, it can be elongated or shortened depending upon the excitation level and frequency. Moreover, the spanwise length of lock-in region will also be measured to realize the interaction between the natural instability waves and the acoustic perturbations.

2. EXPERIMENTAL FACILITY AND DATA PROCESSING

The experiments were conducted in a low-speed, suction-type wind tunnel. The test section of the wind tunnel was 0·2 m wide and 0·4 m high, having a free stream velocity from 3 to 11 m/s with a turbulence intensity of less than 0·5%. A 2-D and three tapered circular models, all manufactured from aluminium alloy rods, were used; the respective dimensions of the models are shown in Figure 1. The span length L of all models is kept at 200 mm so as to fit the entire width of the test section, while all mean diameters $\bar{D}$ are about the same at 20 mm. In most of the cases studied, the operating Reynolds number based on the mean diameter is fixed at $1{\cdot}0 \times 10^4$, and the taper ratios R_T of the models are kept at 40·2. All models used are hollowed inside and have a narrow 0·3 mm wide slot each on the surface. Even though the slot location for emitting acoustic perturbations may be different, the slot length of all models is equal to one mean diameter of the cylinder, which is about one-tenth of the model's span. The acoustic perturbations generated from two 5 W loudspeakers were

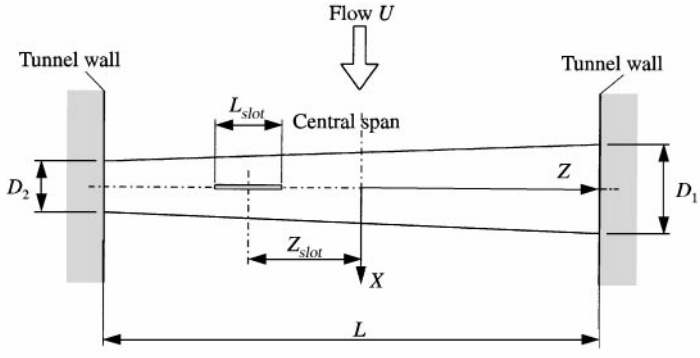

$$\bar{D} = \frac{D_1 + D_2}{2} \qquad R_f = \frac{L}{\bar{D}} \qquad R_T = \frac{L}{D_1 - D_2}$$

(unit: mm)

Model no.	D_1	D_2	$\bar{D}$	L	R_f	R_T	L_{slot}	Z_{slot}
0	20·3	20·3	20·3	200	9·85	∞	20·3	0
1	22·575	17·6	20·0875	200	9·96	40·2	20·1	−80
2								−18·75
3								61·25

Figure 1. Dimensions of circular cylinder models used in the study.

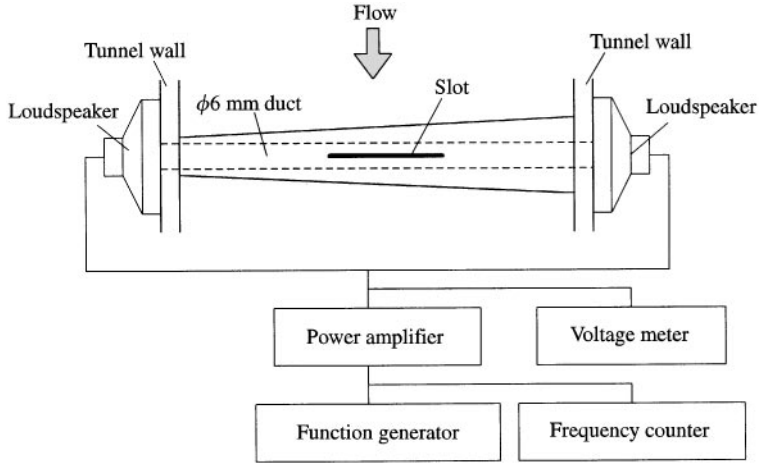

Figure 2. The testing model with a slot and the arrangement of excitation devices.

funneled into the interior of the models from both ends, and then emitted outwards to the flow field through the slot exit. For most of the investigations in this study, the orientation of the slot was placed at 90° from the stagnation point of the cylinder, which has been proved to be the most effective angle of excitation [13]. The block diagram of the excitation system in the experiments is shown in Figure 2.

The Cartesian co-ordinate system is used throughout the investigations, in which the origin is located at the center and the middle span of the cylinder, X-axis along the streamwise direction, Y-axis along the transverse direction, and Z-axis along the spanwise

direction. It is noted that the narrow end of the tapered cylinder is in the negative Z direction, and the wide end in the positive Z direction.

Two constant-temperature anemometers with single or X-typed Platinum hot-wire probe of 5 μm diameter were employed as sensing elements to measure the streamwise and transverse velocities around the wake region. The hot-wire signals were directly digitized by a 16-bit DAP-2400 A/D coverter and then stored and processed by a personal computer. The movement of the probe was done by using a computer-controlled, 2-D traversing mechanism, which can be driven in accuracy of up to 0·025 mm per step.

3. RESULTS AND DISCUSSION

3.1. CELLULAR DISTRIBUTION OF VORTEX-SHEDDING FREQUENCIES

The distributions of natural vortex-shedding frequencies for the tapered model without excitation at $\mathrm{Re}_{\bar{D}} = 5 \times 10^3$ and 1×10^4 in various downstream locations are shown in Figure 3. The shedding frequencies are normalized as either Strouhal number $\mathrm{St}_{\bar{D}}$ based on the mean diameter $\bar{D}$, which appears to be constant inside a cell, or Strouhal number $\mathrm{St}_{\bar{D}}$ based on the local diameter D, which varies linearly inside a cell. This is a vivid example of the cellular structure distribution, or called vortex cells in the wake, as what Gaster [1, 2]

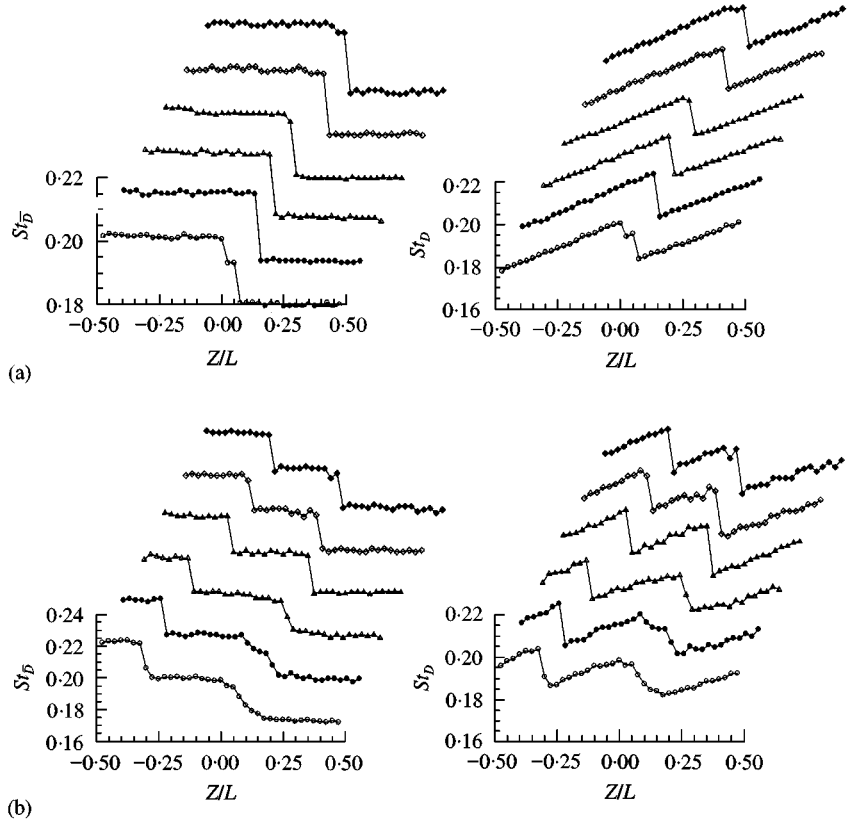

Figure 3. Spanwise distribution of Strouhal numbers based on mean diameter $\bar{D}$ and local diameter D for $R_T = 40{\cdot}2$ at (a) $\mathrm{Re}_{\bar{D}} = 5 \times 10^3$ and (b) $\mathrm{Re}_{\bar{D}} = 1 \times 10^4$. ⊖ 2; ● 3; △ 5; ▲ 10; ◇ 15; ◆ 20.

first found. In the present study, two vortex cells were obtained for $\mathrm{Re}_{\bar{D}} = 5 \times 10^3$ and three for 1×10^4, as shown in Figure 3. For more details, see reference [10].

It is shown in Figure 3 that the shedding-frequency distributions are all cellular in the downstream locations measured, and the number of cells remains the same as that at $X/\bar{D} = 2$. In addition, the length of the left cell at the narrow end (negative Z-axis) of the cylinder slightly elongates for $\mathrm{Re}_{\bar{D}} = 1 \times 10^4$ when $X/\bar{D} \geqslant 10$, and the frequency jump between cells becomes steeper and shorter in the downstream. However, the cellular distributions of the vortex-shedding frequencies as a whole have no significant change in the wake region even up to $X/\bar{D} = 20$.

The typical result, shown in Figure 3, of the vortex-shedding frequency distributions along the spanwise direction in the wake indicates that the formation of the vortical structures in the downstream has just completed in the near wake region before $X/\bar{D} < 2$ in the Reynolds number range operated. This can be further substantiated by the numerical simulation of Jespersen and Levit [14] and the flow visualization study of Piccirillo and Van Atta [15] in the low Reynolds number wake flow. Both results clearly demonstrated that the cellular vortical structures were formed in accordance with the roll-up of the shedding vortices right behind the cylinder. The occurrence of spanwise coupling in the intersection of the shedding frequencies, or frequency jump, especially warrants more thorough investigation into its effect on the cellular structures in the wake behind a 2-D circular or tapered circular cylinder.

3.2. SPANWISE COUPLING OF CELLULAR STRUCTURES BEHIND 2-D CIRCULAR CYLINDER

The wake flow behind a 2-D circular cylinder is first examined to investigate the spanwise coupling on the cellular structures of the shedding vortices. Although the 2-D circular cylinder may generate the cellular distribution of shedding frequencies in such special cases as are due to the end effect in a 2-D cylinder wake [4, 5] and the non-uniformity of the oncoming flow [6], the distribution of the natural shedding frequencies behind the 2-D circular cylinder in the present facility has been found to be regular and uniform. It is noted that, by introducing acoustic perturbation to the flow field through a slot on the surface of the cylinder [3], the uniform shedding-frequency distribution could be artificially made to become cellular distribution with different excitation frequencies from their natural ones. In the mean time, this effect is very sensitive to the excitation frequency and level applied. Because both the frequency and the level of the perturbations are easy to adjust, they can even be used as control parameters to investigate the spanwise coupling on the cellular distribution of the shedding frequencies.

In the experimental facility used here, the acoustic perturbations were generated by two loudspeakers, respectively, located at both ends of the cylinder, and the excitation level was defined as the peak value of the exit velocity, denoted by u_p, at the slot exit when no flow operated. This follows the suggestion made by Chang *et al.* [16] that u_p is a good parameter to represent the excitation level. The typical time traces shown in Figure 4 correspond to the exit velocities detected by a single-typed hot-wire probe placed at the slot exit where there was no free stream velocity. Because the hot-wire sensor cannot distinguish the flow directions, the negative velocity in the reversed suction phase was sensed to be positive. However, only the maximum peak values in the injection phase were counted to define the excitation level, u_p, which is usually dependent upon the driven voltage and frequency, f_e, of the loudspeakers. Thus, the calibrations of u_p with respect to these two parameters were performed in advance before proceeding with the experiments. In addition, the spanwise non-uniformity of the excitation level at the slot was measured to be less than 1%.

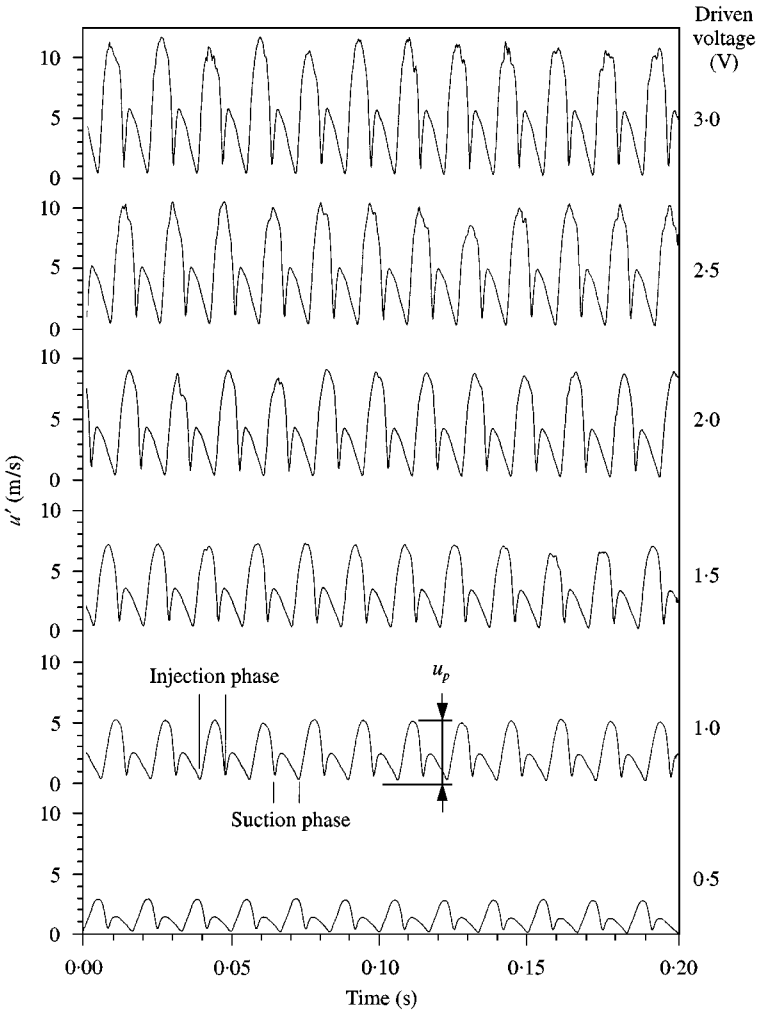

Figure 4. Time traces of the exit velocity at the slot for $f_e = 60$ Hz when there is no free stream velocity.

There is consensus that the existence of the slot itself may perturb (or trip) the flow field even without introducing the acoustic perturbations. To begin with the experiments, the degree of influence due to the slot tripping was tested. Figure 5 presents such a case of the energy spectra of the transverse velocity fluctuations at $X/D = 2$, $Y/D = 0{\cdot}5$ and $Z/L = 0$, which was located at the central span of the 2-D cylinder with and without the slot. The data shows that the existence of the slot reveals some effects on the energy spectra; for instance, the first-harmonic frequency of the shedding vortices disappears and the spectral energy of the vortex-shedding frequency slightly decreases as well as the frequency band spreading leftward to the low-frequency side. Nevertheless, the shedding frequency remains at the same peak and is not affected at all.

According to the study of Wei and Smith [17] for the uniform flow passing a 2-D circular cylinder placed in the cross-stream direction, the laminar boundary layer over the cylinder surface is formed and then separated from the surface to form a stream of shear layers. These unstable shear layers will roll up into small eddies due to Kelvin–Helmholtz instability. These eddies then accumulate their energy to form the large-scaled vortices and

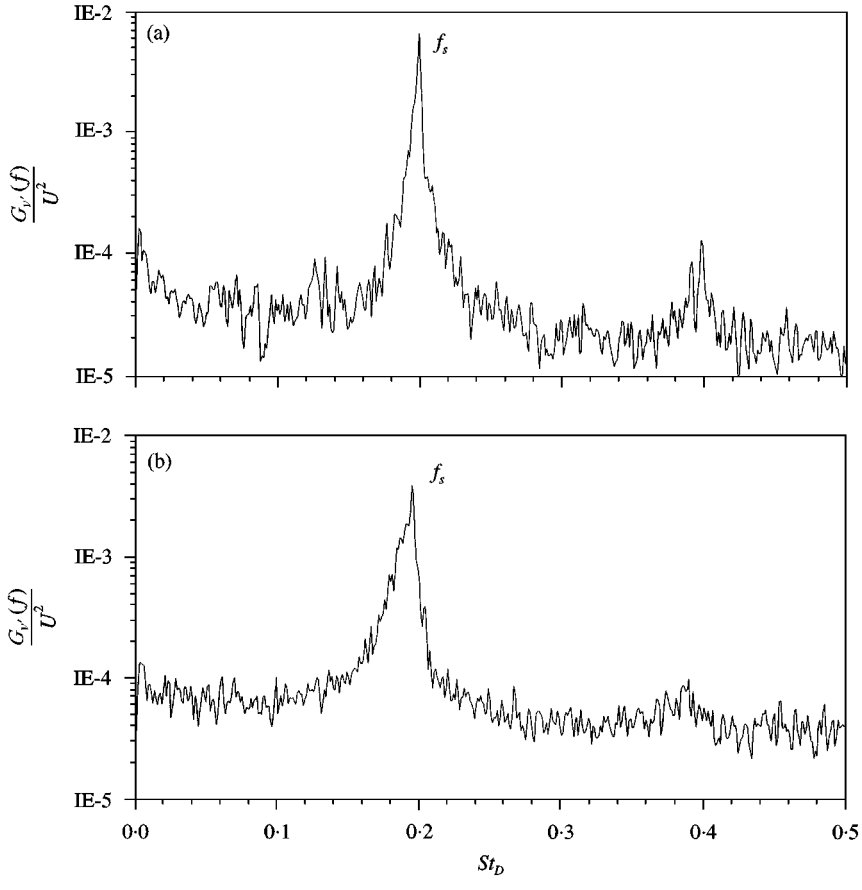

Figure 5. Energy spectra of transverse velocity fluctuations for the 2-D circular cylinder at the middle span and $X/D = 2$, $Y/D = 0{\cdot}5$: (a) without the slot, (b) with the slot at 90° from the front stagnation point.

subsequently shed into the wake with a specific frequency. When perturbations for excitation were introduced at the same frequency of the shedding vortices, $f_e = f_s$, the process of energy accumulation to form the large-scaled vortices was accelerated and the shedding vortex structures became more organized. Therefore, the energy content of the shedding vortices after excitation shown in Figure 6 is more concentrated than the natural case without excitation. In addition, the energy content of the concentrated peak increases with the increase in excitation level. On the other hand, when the excitation frequency used is different from the shedding frequency, $f_e \neq f_s$, these two frequencies may co-exist in the energy spectra, as shown in Figure 7. When the excitation level applied is not high as in the case in Figure 7(b), the natural vortex-shedding frequency still prevails in the spectra. However, the energy content of f_e will override the natural one if the excitation level is high enough (Figure 7(c)), which is the case where the vortex shedding is locked into the excitation frequency instead of the natural shedding frequency.

Both natural and excitation frequencies have the same opportunity to become dominant in the flow field, but they are strongly related to the level of the perturbations introduced. Figure 8 presents the results of the dominant frequency, called the response frequency f_r, measured at the central span with different excitation frequencies and levels. When the response frequency equals the natural shedding frequency, i.e., $f_r/f_s = 1$, this is the usual

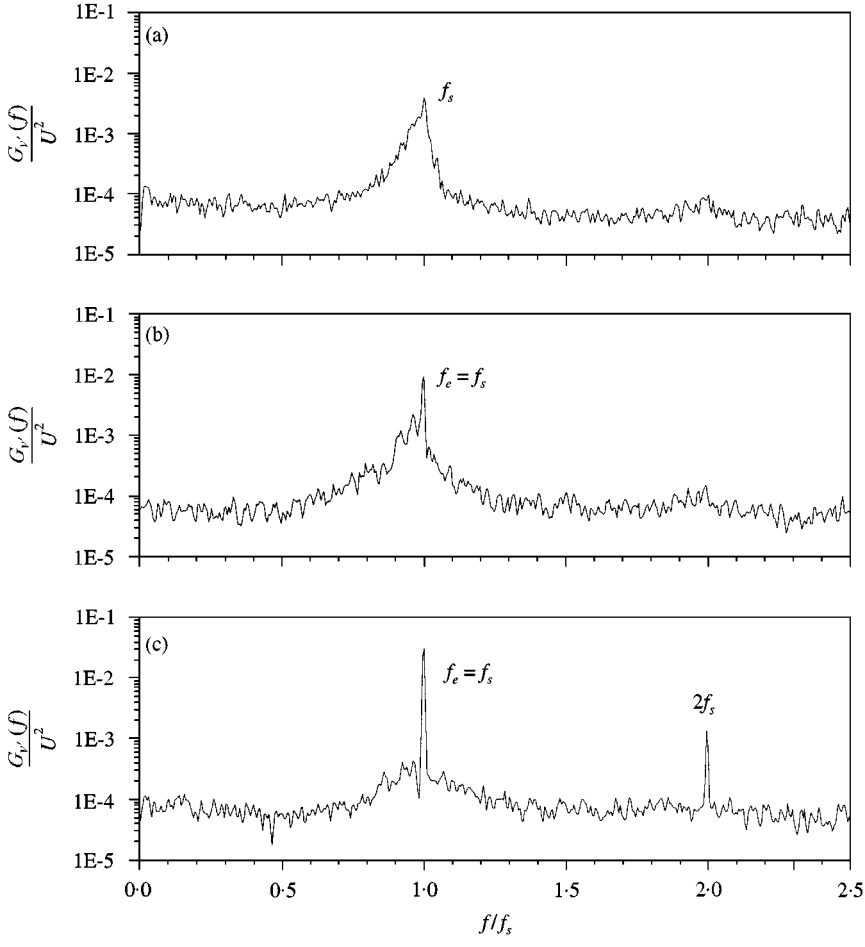

Figure 6. Energy spectra of transverse velocity fluctuations for the 2-D circular cylinder at the middle span and $X/D = 2$, $Y/D = 0{\cdot}5$: (a) without excitation; and with excitations of $f_e/f_s = 1$ and driven voltage equals, (b) 1·0 v, (c) 2·0 V.

case where the excitation can effectively enhance the natural shedding vortices. When the level of excitation increases in conjunction with the excitation frequency, the response frequency will follow the linearly slanted behavior as shown in Figure 8, which stands for the occurrence of vortex lock-in. In terms of the excitation frequency and level used, three lock-in regions are clearly observed, as shown in Figure 9, where these three regions with corresponding conditions of $f_e/f_s = 1$, 2, and 0·5 are labelled as Regions I, II and III respectively. Clearly, Region I presents the most significant region corresponding to the fundamental mode excitation, which contains the condition of $f_e/f_s = 1$. Region II takes place around the condition of $f_e/f_s = 0{\cdot}5$, namely the sub-harmonic mode excitation, where the ratio of the response frequency to the excitation frequency, f_r/f_e, is 2. Region III includes the condition of $f_e/f_s = 2$ or the first-harmonic mode excitation, in which $f_r/f_e = 0{\cdot}5$.

Two important properties of the lock-in phenomenon are worth noting. One is the dependence of the required excitation level on producing the difference between the excitation frequency and the natural shedding frequency. That is, the required excitation

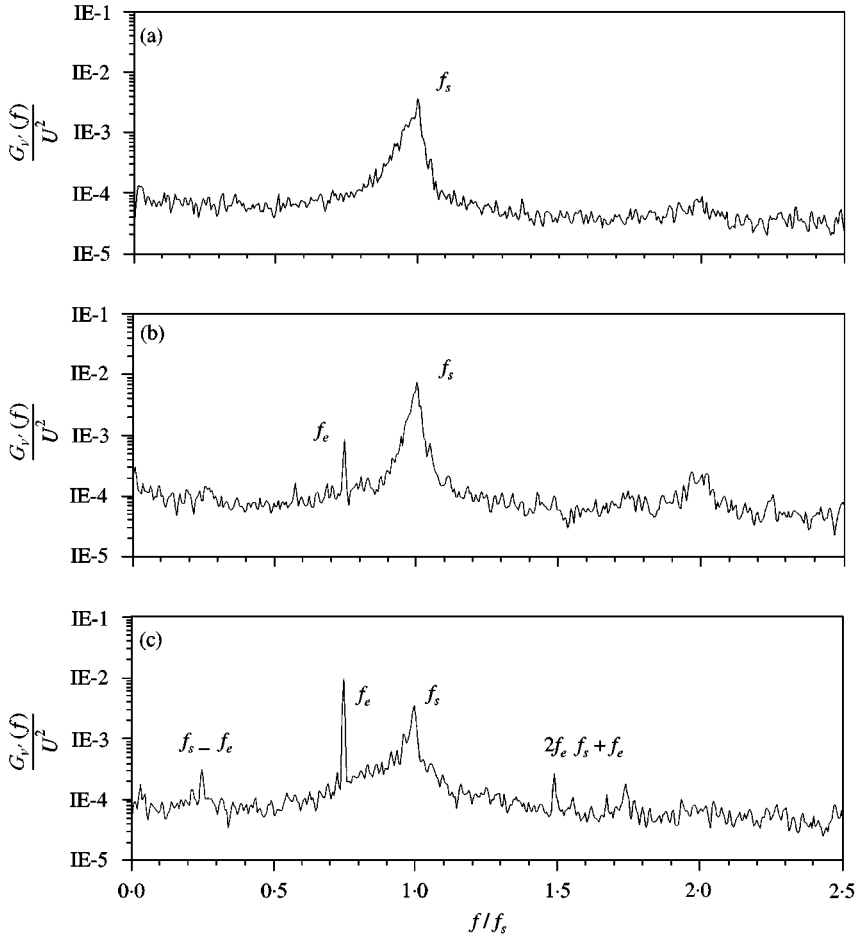

Figure 7. Energy spectra of transverse velocity fluctuations for the 2-D circular cylinder at the middle span and $X/D = 2$, $Y/D = 0{\cdot}5$: (a) without excitation; and with excitations of $f_e/f_s = 0{\cdot}75$ and driven voltage equals, (b) 1·0 v, (c) 2·0 V.

level is higher when the difference between the frequencies is increased. The other is the asymmetry of the lock-in region with respect to the reference mode. For instance, the required excitation level in Region I ($f_r/f_e = 1$) to lock in the shedding vortex on the left-hand side ($f_e/f_s < 1$) is smaller than that on the right-hand side ($f_e/f_s > 1$), provided the difference of f_e and f_s is identical. The same result occurs in Regions II and III. These two properties have also been witnessed in the study of the shedding vortex lock-in phenomenon through the cylinder vibration in the bluff body wakes by Griffin and Hall [11].

The effect of acoustic excitation on the shedding frequencies along the span is illustrated in Figure 10, in which the excitation frequency is diffferent from the natural one, i.e., $f_e/f_s = 0{\cdot}86$. The spanwise distribution of the Strouhal number based on the dominant frequencies is shown in Figure 10(a). It is noted that the response frequency is locked into the excitation frequency in the region between $Z/L = 0$ and 0·14, although the slot extends only to about $Z/L = 0{\cdot}05$. Several relevant energy spectra at $Z/L = 0$, 0·14, 0·15 and 0·3 are, respectively, illustrated in Figure 10(b). In the middle of the cylinder, $Z/L = 0$, the excitation frequency is clearly dominant in comparison with the shedding frequency f_s. When the

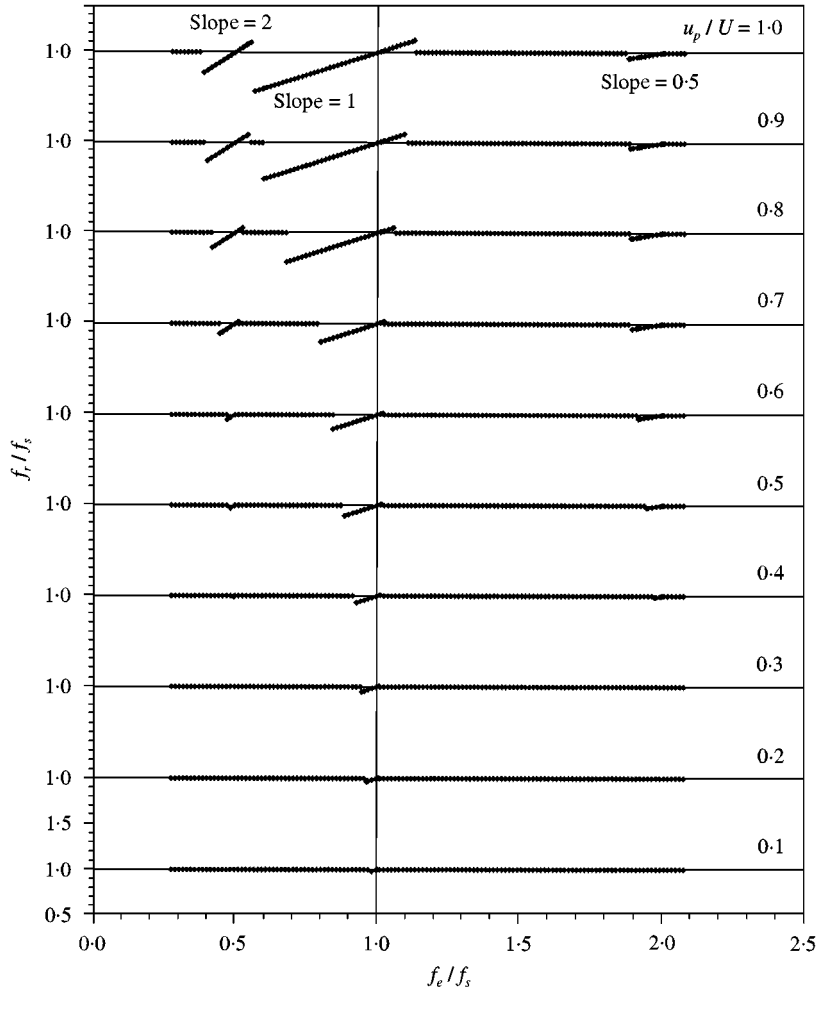

Figure 8. Response frequencies at the middle span of the 2-D circular cylinder with various excitation levels.

measuring point moves away from the slot center, $Z/L > 0$, the spectral energy of the excitation frequency keeps decreasing while that of the natural shedding frequency increases accordingly. When $Z/L > 0{\cdot}14$, i.e., moving farther away from the slot, the natural shedding frequency reverts to being dominant. During the intersection of the frequency jump around $Z/L = 0{\cdot}14$. However, it is reversed at around $Z/L = 0{\cdot}15$ where f_s becomes dominant. Hence, the boundary of the frequency jump between cells is determined to be at $Z/L = 0{\cdot}145$. The difference between the spectral energy peaks of f_e and f_s appears more evident at $Z/L = 0{\cdot}3$. It is noted in Figure 10(a) that only the half-span of the measuremnts is depicted and the lock-in region occurs between $Z/L = \pm 0{\cdot}145$. Therefore, the lock-in length, denoted as L_{lock}, is $0{\cdot}29\,L$ in this excitation condition.

The evolution of the energy spectra along the span is very similar to the evolution when the excitation level is decreasing. The analogy of the influences between the excitation level and the spanwise location indicates that the perturbations emitted from the slot, which spans $Z/L = -0{\cdot}05075$ and $+0{\cdot}05075$, propagate to the left and right along the span, while the measured spectral energy of the excitation frequency decays when the measuring

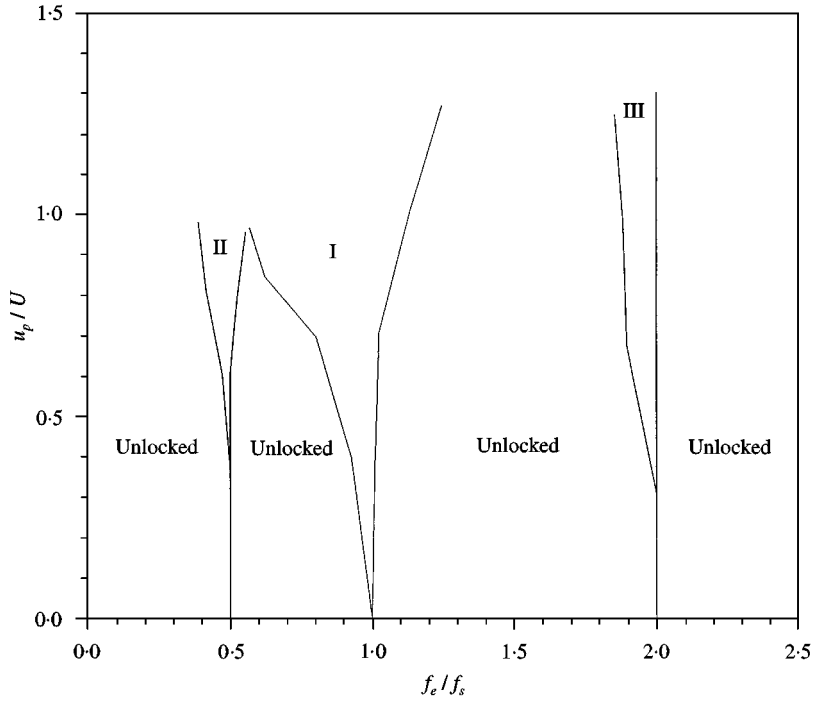

Figure 9. Lock-in region referred to the response frequencies at the middle span of the 2-D circular cylinder under excitation. Region I, $f_r/f_e = 1$; II, $f_r/f_e = 2$; III, $f_r/f_e = 0{\cdot}5$.

point moves farther away from the slot. The interaction due to the spanwise coupling between the local instability waves and the perturbations from the slot concurrently determines which will respond to the vortex-shedding frequency. This result facilitates the determination of the vortex lock-in due to the spanwise coupling in the cellular distribution of the shedding frequencies.

The spanwise lock-in length in Region I ($f_r/f_e = 1$) is extensively measured at various excitation levels and frequencies for the 2-D circular cylinder, which is shown in Figure 11. As expected, the result is obviously asymmetric to the condition $f_e/f_s = 1$, and the influence of the acoustic excitation in $f_e < f_s$ expands wider than that in $f_e > f_s$. However, the lock-in length spans longer when the difference of the excitation frequency and the natural shedding frequency is less and the excitation level is higher.

3.3. INFLUENCE OF EXCITATION ON SPANWISE COUPLING IN TAPERED CIRCULAR CYLINDER WAKE

The results in the previous section have demonstrated that the acoustic perturbations emitted from the partial span of the 2-D cylinder have shown significant influence on the spanwise coupling of the shedding vortices in the wake. The spanwise coupling of the votex-shedding frequencies behind the tapered circular cylinder was also examined here by arranging the slot locations at $Z_{slot}/L = 0{\cdot}4$, $-0{\cdot}0938$ and $0{\cdot}3063$, which correspond to the respective centers of the constant-frequency cells in the tapered cylinder wake without excitation [10]. Again, before conducting the experiments, the calibration of the excitation

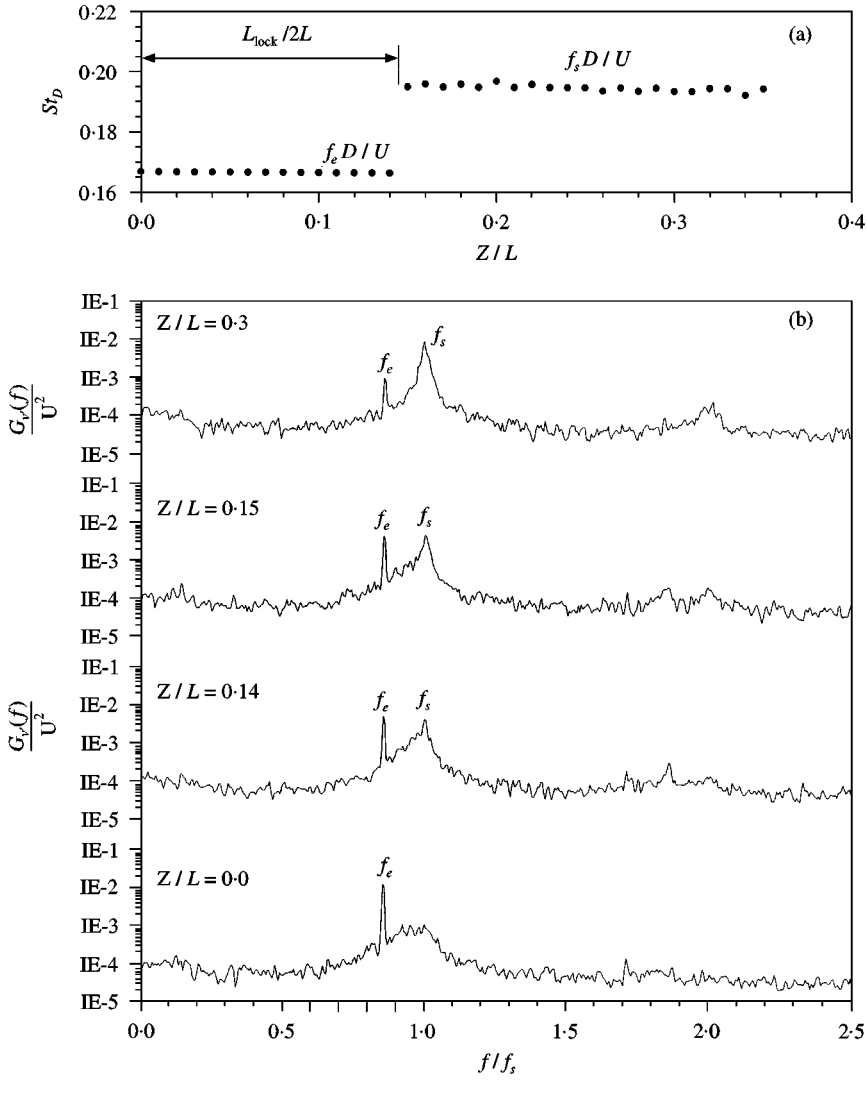

Figure 10. (a) Spanwise distribution of St_D for the 2-D circular cylinder under excitation of $f_e = 62$ Hz ($0{\cdot}86f_s$) and $u_p/U = 0{\cdot}97$, and (b) the corresponding spectra at various spanwise locations.

level u_p at the slot exit with respect to the driven voltage and frequency of the loudspeakers was also performed in advance.

The effects of the slot position and the slot orientation on the shedding vortices were first investigated. As opposed to the results for the 2-D cylinder in the previous section, the existence of the slot may have significant effects on the distribution of the vortex-shedding frequencies. The degree of influence on the $St_{\bar{D}}$ distribution for the three slot locations was not the same, as shown in Figures 12–14.

Figure 12(a) presents the comparison of $St_{\bar{D}}$ along the span without the slot and with the slot located at $Z_{slot}/L = 0{\cdot}3063$ and oriented 90° from the front stagnation point. The shedding frequencies corresponding to the three cells measured in the case without the slot are denoted as f_1, f_2, and f_3. It is noted that the effect of the slot located at $Z_{slot}/L = 0{\cdot}3063$ on the $St_{\bar{D}}$ distribution is not significant. Although the boundaries of cells are shifted a little,

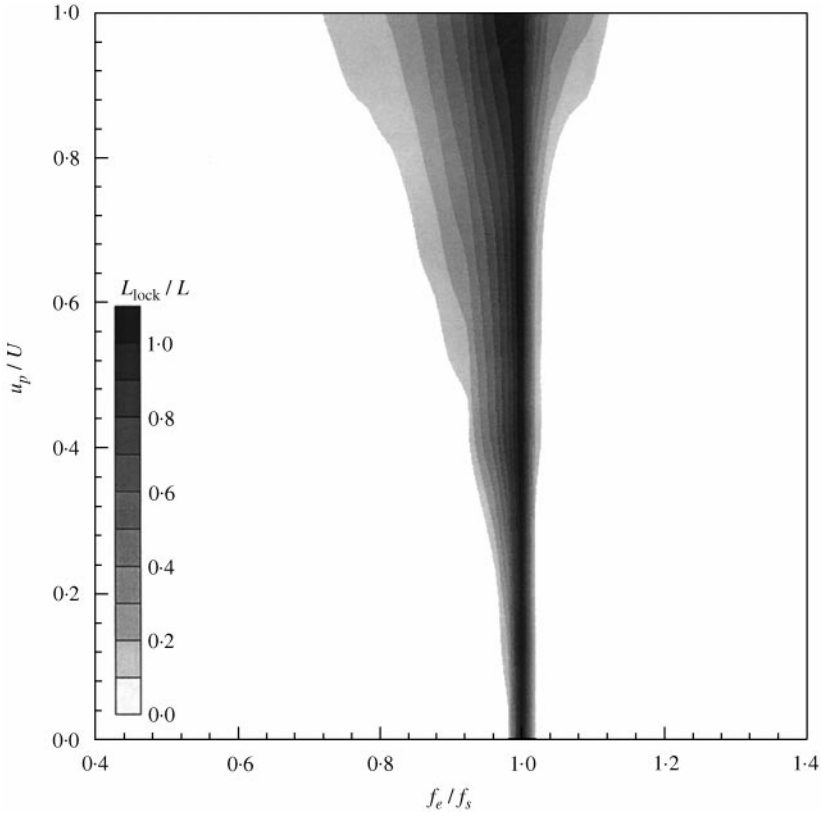

Figure 11. Lock-in length spreading at various excitation frequencies and levels for the 2-D circular cylinder.

the intersection region between f_1 and f_2 cells is clearly shortened, indicating that the cellular structure becomes more well defined. To further substantiate the influence of the slot, several slot orientations from 0 to 180° were tested. As shown in Figure 12(b), the effect of the slot at various angles is not promising for the excitation case $Z_{slot}/L = 0{\cdot}3063$.

However, the effect of the slot located at $Z_{slot}/L = -0{\cdot}0938$ on the distribution of $St_{\bar{D}}$ is more significant than that of the slot at $Z_{slot}/L = 0{\cdot}3063$, as shown in Figure 13(a). Although the existence of the slot has already affected the dominant peaks of the central cell and the boundaries of the left and right cells, the dominant frequencies f_1 and f_3 cells still remain about the same. As shown in Figure 13(b), the slot does not affect the distribution of $St_{\bar{D}}$ except that it is oriented between 90 and 60°, which is within the flow separation region.

When the slot is located at $Z_{slot}/L = -0{\cdot}4$ as shown in Figure 14(a), the right cell with the shedding frequency f_1 is barely influenced but the left and middle cells are dramatically altered. A new left cell, which is longer and has a dominant frequency approximately at the average of f_2 and f_3, is extended from the narrow end to roughly $Z/L = -0{\cdot}1$. When the slot is oriented between 90 and 60°, the alteration of the distribution of the $St_{\bar{D}}$ also occurs as illustrated in Figure 14(b).

Although the spanwise distribution of the shedding frequencies in the tapered cylinder wake may be affected due to the slot orientation with respect to the flow direction as discussed above, the present study concentrates on the spanwise coupling of the shedding

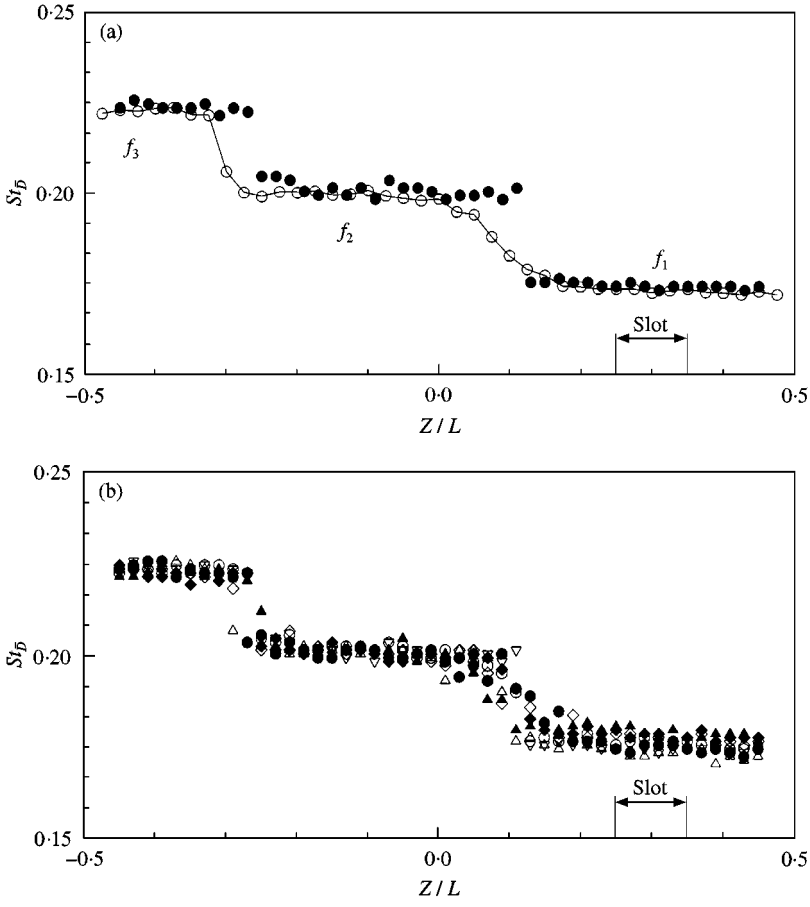

Figure 12. (a) Comparisons of St_D-distribution with slot at 90° and without the slot: ● with slot at 90°; –○– without slot. (b) Influence of the slot position on St_D-distributions, for the tapered model with $Z_{slot}/L = 0{\cdot}3063$: ○ 0°; ● 30°; △ 60°; ▽90°; ▲ 120°; ◇ 150°; ◆ 180°.

vortices excited by the acoustic perturbations emitted from the slot oriented at 90° and placed at three slot positions along the span. The distributions of St_D are, respectively, shown in Figures 15–17 as well as the corresponding lock-in length. It is noted that the excitation frequency is equal to the natural shedding frequency of the corresponding cell when there is no slot influence. In this study, the lock-in length L_{lock} is defined as the spanwise length of the cell which is firmly locked in to the excitation frequency. By referring to the slot location Z_{slot}, the lock-in length is divided into the left- and right-hand parts with respect to the slot position, which are, respectively, denoted as L^-_{lock} and L^+_{lock}. That is, L^-_{lock} is the distance from the Z_{slot} centre to the left boundary of the lock-in region and L^+_{lock} the distance to the right boundary. It is obvious in Figure 15(a) that the increase in excitation level will effectively elongate the cell size and give rise to more regular distribution of the shedding frequencies, which is also obtaind in the study of the 2-D cylinder wake in the previous section.

As revealed in the Figure 12b, the distribution of the shedding frequencies is clearly not affected by the slot placed at $Z_{slot}/L = 0{\cdot}3063$. Hence, the dominant frequency in the right cell is still f_1 for the absence of the excitation and the lock-in length accordingly equals the original length of the cell, as shown in Figure 15(b). When the excitation level increases to

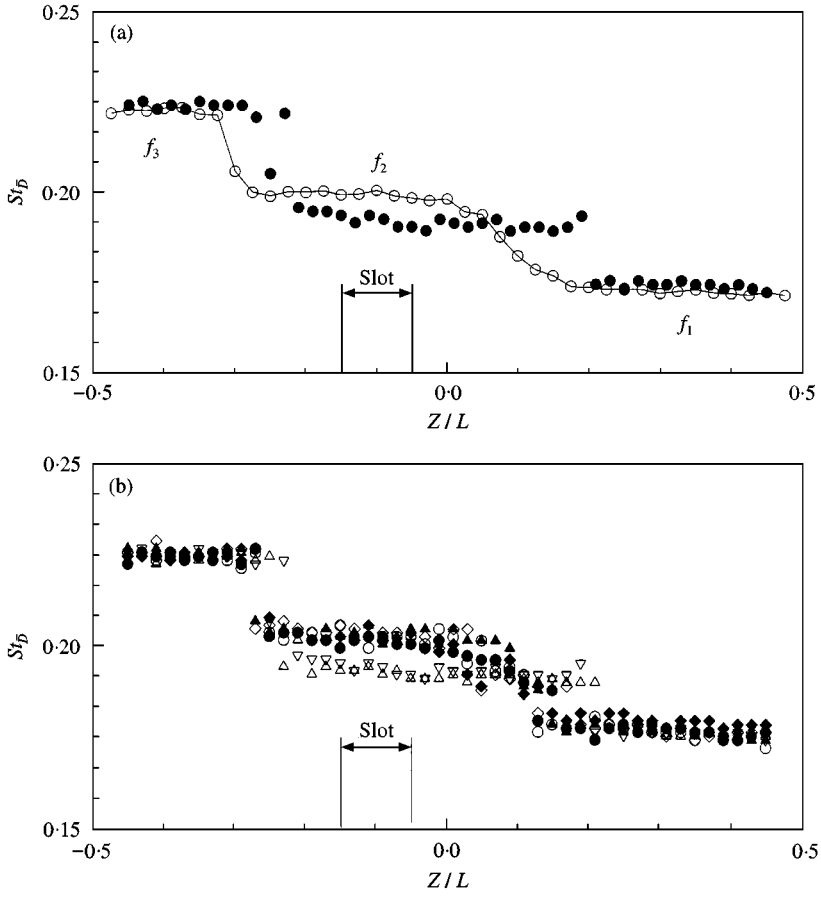

Figure 13. Comparisons of $St_{\bar{D}}$-distribution with slot at 90° and without the slot: ● with slot at 90°; —○— without slot. (b) Influence of the slot position on $St_{\bar{D}}$-distributions, for the tapered model with $Z_{slot}/L = -0{\cdot}0938$: ○ 0°; ● 30°; △ 60°; ▽ 90°; ▲ 120°; ◇ 150°; ◆ 180°.

$u_p/U = 0{\cdot}20$, the lock-in region does not elongate very much but the distribution of $St_{\bar{D}}$ becomes more regular. The lock-in region extends leftward when the excitation level increases (Figure 15(a)), while the right cell always extends to the extreme end of the tapered cylinder and the value of L^+_{lock} always remains constant. The left-hand side lock-in length extends very mildly when $u_p/U \geqslant 0{\cdot}69$ and obtains saturation at $u_p/U = 1{\cdot}39$. That is, the saturated value of L^-_{lock} is 0·346. It s noted that the left cell adjacent to the narrow end is not much affected by the excitation, but the central cell is shortened due to the extension of the left-hand lock-in region.

For the case of $Z_{slot}/L = -0{\cdot}0938$ where the excitation frequency is equal to the original shedding frequency f_2 of the central cell and the excitation level is large enough, a restored cell is obtained, as shown in Figure 16. Especially, when $u_p/U = 0{\cdot}62$ is employed, the central cell having the frequency f_2 is completely restored. In addition, the extension of the central cell to the right-hand side is saturated when $u_p/U = 1{\cdot}11$, while the leftward extension continues until $u_p/U = 1{\cdot}34$. The saturated vlaues of L^+_{lock} and L^-_{lock} are 0·346 and 0·274 respectively. It is noted that the left-hand lock-in length L^-_{lock} is always longer than the right-hand lock-in length L^+_{lock} although they are nearly equal when u_p/U ranges from 0·62 to 1·27. This is in agreement with the results in Figures 9 and 11, which suggests that the

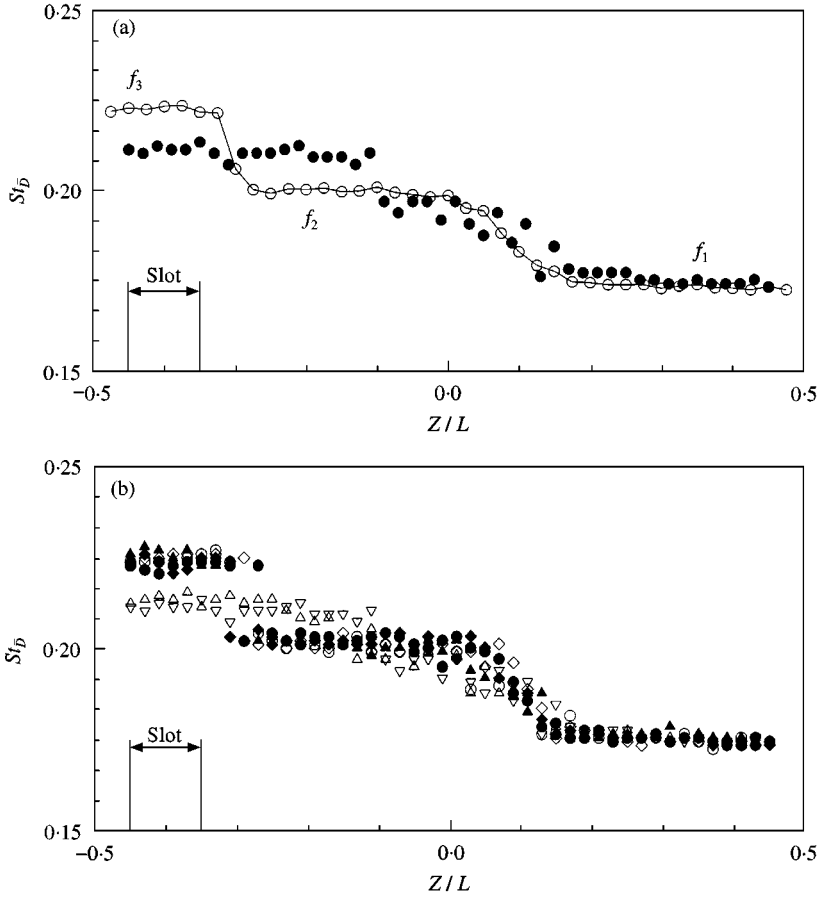

Figure 14. Comparisons of $St_{\bar{D}}$-distribution with slot at 90° and without the slot: ● with slot at 90°; —○— without slot. (b) Influence of the slot position on $St_{\bar{D}}$-distributions, for the tapered model with $Z_{slot}/L = -0{\cdot}4$: ○ 0°; ● 30°; △ 60°; ▽ 90°; ▲ 120°; ◇ 150°; ◆ 180°.

excitation frequency applied lower than the natural frequency affects the vortex shedding more easily than the excitation frequency applied higher than the natural frequency. In the tapered cylinder with the slot at $Z_{slot}/L = -0{\cdot}0938$ in the present case, the excitation frequency f_2 is lower than f_3 but higher than f_1. Therefore, the excitation of the wake at the frequency f_2 affects the left-hand cell, more significantly the right-hand cell.

In the case of $Z_{slot}/L = -0{\cdot}4$ as shown in Figure 17, the left-hand side and central cells are already altered because of the slot tripping to modify the most unstable waves in the wake, even though no excitation is applied. However, excitation at the original shedding frequency f_3 seems to reconstruct the cell, especially when the excitation level is increased to $u_p/U = 0{\cdot}67$. Meanwhile, the left-hand cell length is elongated with the increase of u_p/U. Although the excitation is only introduced at the natural shedding frequency f_3 of the left-hand cell, the central cell with frequency f_2 remains unchanged in the natural case without excitation. When the excitation level at frequency f_3 is large enough to override the natural instability waves, the excitation at frequency f_3 will play the same and major role as the original instability waves of f_3. This can explain why the original distribution of the

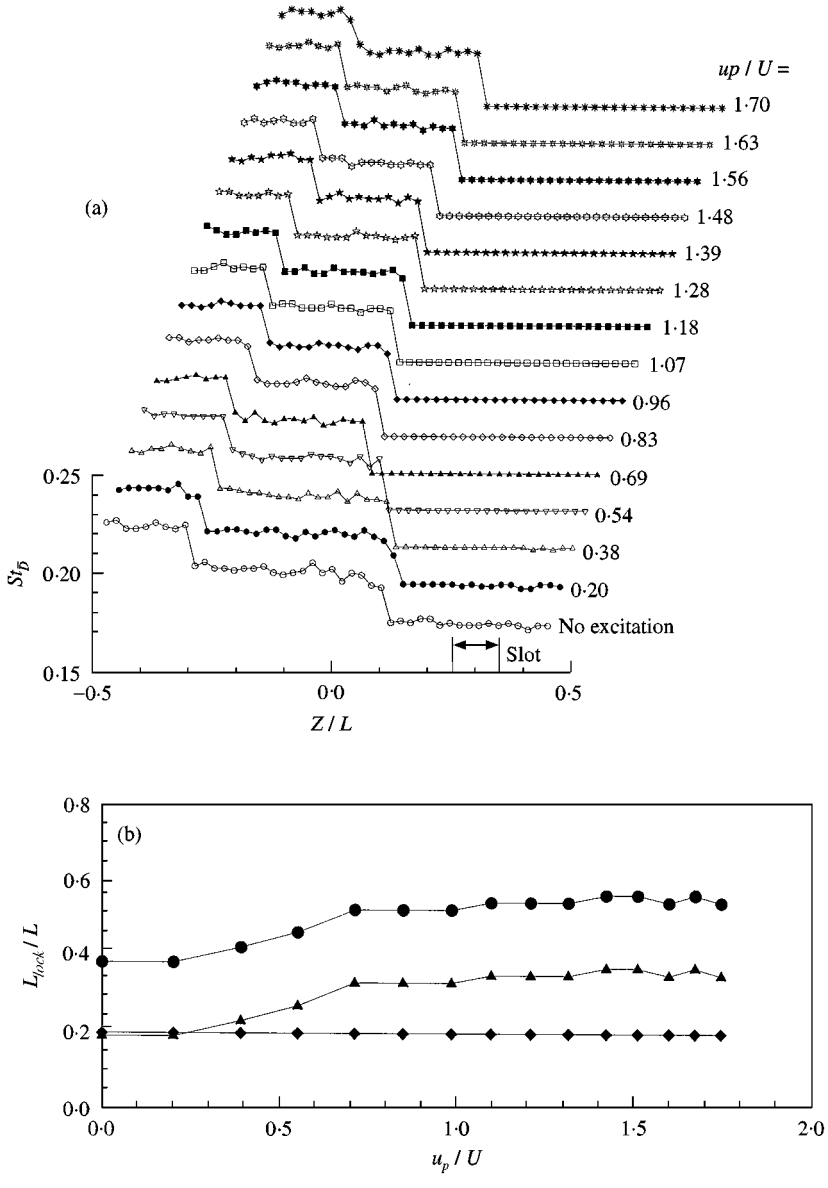

Figure 15. (a) Distributions of $St_{\bar{D}}$ and (b) the lock-in length for various excitation levels with the slot located at $Z_{slot}/L = 0{\cdot}3063$ and 90°: –▲– L^{-}_{lock}/L; –◆– L^{+}_{lock}/L; –●– L_{lock}/L.

shedding frequencies is restored after the excitation is introduced. These results also demonstrate that, with regard to the cell formation process, the acoustic perturbations used for excitation can be equivalent to the instability waves inherently embedded in the natural wake flow. Hence, it is adequate to explain the spanwise coupling mechanism based on the spanwise propagation and interaction of instability waves, as proposed by Hsiao and Chiang [10].

With the increase in excitation level, the lock-in region will elongate accordingly until it reaches a saturation value when $u_p/U > 0{\cdot}49$, as shown in Figure 17(b). However, the

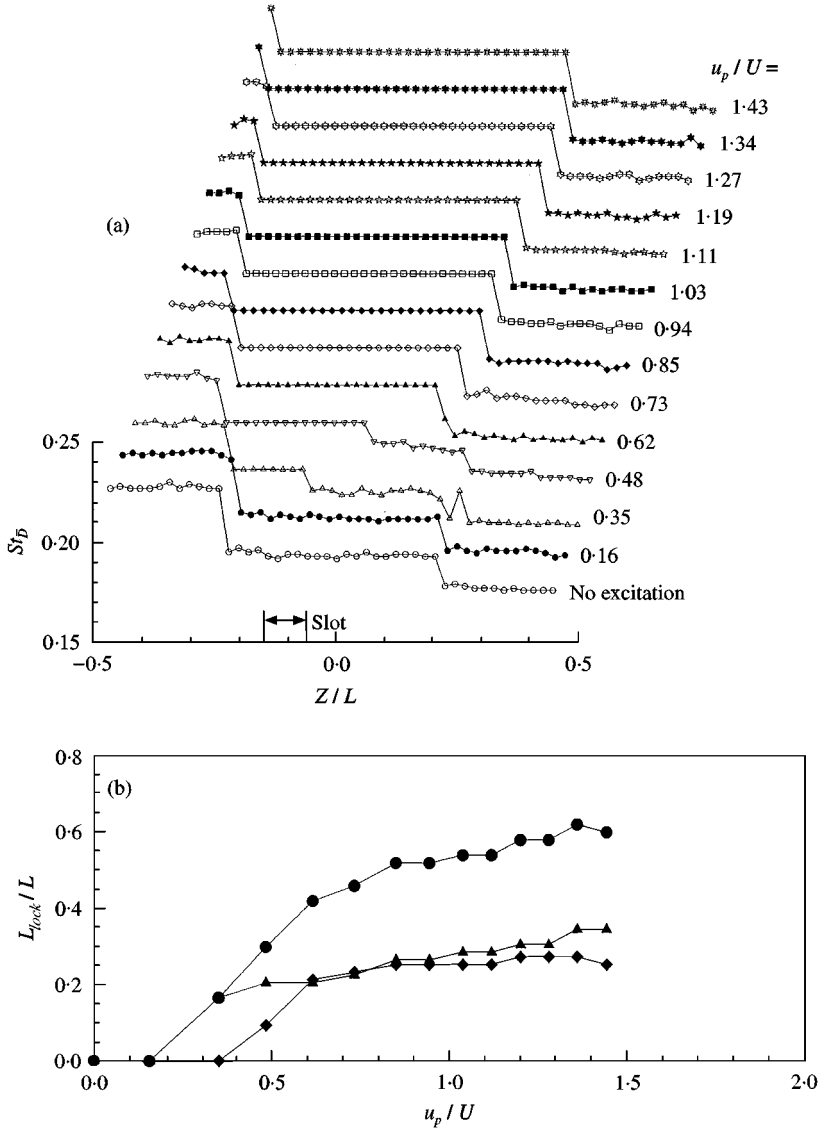

Figure 16. (a) Distributions of St_D and (b) the lock-in length for various excitation levels with the slot located at $Z_{slot}/L = -0{\cdot}0938$ and 90°: –▲– L^-_{lock}/L; –◆– L^+_{lock}/L; –●– L_{lock}/L.

lock-in region extends leftward to the narrow end of the tapered cylinder when $u_p/U \geqslant 0{\cdot}67$; its extension to the right ceases to increase at $L^+_{lock} = 0{\cdot}28$ when $u_p/U \geqslant 1{\cdot}31$, but never reaches the wide end of the cylinder. The experimental results with the slot oriented at 120° are concurrently shown in Figure 17(b), where the spanwise distribution of the $St_{\bar{D}}$ is not affected by the slot, and the lock-in length for the small excitation level is not zero. The excitation with the slot at 120° is also saturated at the same excitation level.

The saturation values of the lock-in length and the corresponding required excitation levels for the spanwise coupling in the lock-in region were also measured at three slot locations, which were collected in Table 1 for comparison. Data show that the saturated

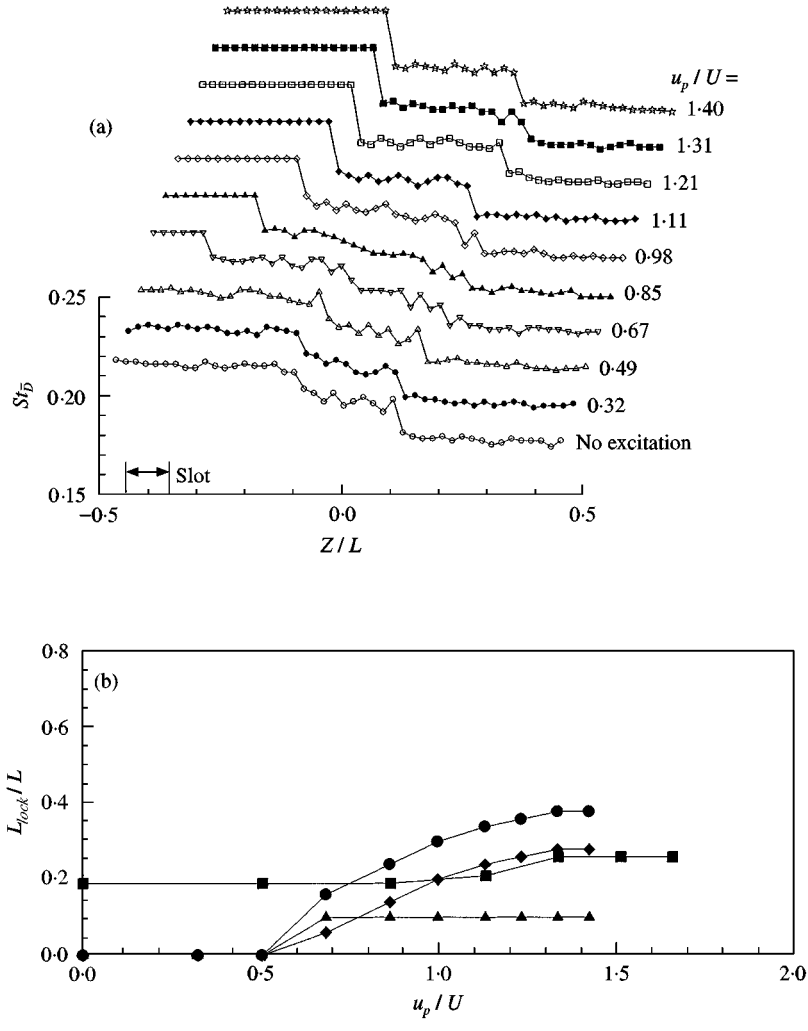

Figure 17. (a) Distributions of $St_{\bar{D}}$ and (b) the lock-in length for various excitation levels with the slot located at $Z_{slot}/L = -0{\cdot}4$ and 90°: –▲– L^{-}_{lock}/L; –◆– L^{+}_{lock}/L; –●– L_{lock}/L; –■– L_{lock}/L (slot at 120°).

TABLE 1

Saturated lock-in length and minimum required excitation level to reach the saturation

Z_{slot}/L	Saturated lock-in length			Minimum required (u_p/U)		
	L^{-}_{lock}	L^{+}_{lock}	L_{lock}	L^{-}_{lock}	L^{+}_{lock}	L_{lock}
−0·4	Narrow end	0·28	0·38	Narrow end	1·31	1·31
−0·0938	0·346	0·274	0·62	1·34	1·11	1·34
0·3063	0·346	Wide end	0·54	1·39	Wide end	1·39

values of L^{-}_{lock} and L^{+}_{lock} almost remain the same for different slot locations, although the respective minimum required excitation levels to generate the saturation are not the same. Because of the spanwise coupling between cells in the wake, it is not difficult to modify the cellular formation of the shedding frequencies in the 3-D tapered cylinder wake in becoming

the uniform distribution for the 2-D cylinder wake under the maximum excitation level applied in the present study.

4. CONCLUDING REMARKS

The spanwise coupling of the shedding vortices under acoustic excitation in the turbulent wake behind a 2-D and a tapered circular cylinder was experimentally studied by means of hot-wire measurements in a low-speed wind tunnel. The spanwise propagation and interaction of the shedding vortices between the cellular structures were clearly investigated by exciting the shedding vortices at relevant excitation frequencies and levels of the acoustic waves emitted from a narrow slot placed at various positions and orientations from the front stagnation point of the model.

For the wake behind the 2-D circular cylinder, the shedding vortex structures were strongly enhanced due to the acoustic excitation at its original vortex-shedding frequency. The shedding vortices were faithfully locked into the excitation frequency when a high level of excitation was employed. With regard to the excitation level applied, three lock-in regions corresponding to the ratio of the response frequency to the excitation frequency were obtained; that is, $f_r/f_e = 1$, 2, and 0·5. In addition, the excitation case of $f_e < f_s$ is easier to lock in the shedding vortices than that of $f_e > f_s$. Meanwhile, it is possible to generate the spanwise cellular distribution of the shedding frequencies in the 2-D cylinder wake, especially when the excitation is applied. The acoustic perturbations emitted from the slot could propagate along the spanwise direction, but their energy decays as they move further downstream.

For the wake behind the tapered cylinder, the original distribution of the shedding frequencies may be significantly altered due to slot tripping. After the wake was excited at the natural shedding frequency, the original cell formation was restored when the excitation level was large enough. Not only was the excited cell affected, but also the adjacent cells. The length of the lock-in region extending to the left or to the right from the excitation slot would reach a saturation value. In addition, the saturated length of the left-hand lock-in region when close to the narrow end of the tapered cylinder was almost identical for three slot locations of excitation. Similar results also occur for the saturated length of the right-hand lock-in region close to the wide end cylinder. Nevertheless, the minimum required excitation levels for both to generate the saturated values were not identical.

REFERENCES

1. M. GASTER 1969 *Journal of Fluid Mechanics* **38**, 565–576. Vortex shedding from slender cones at low Reynolds numbers.
2. M. GASTER 1971 *Journal of Fluid Mechanics* **46**, 749–756. Vortex shedding from circular cylinders at low Reynolds numbers.
3. F. B. HSIAO, J. Y. PAN and C. H. CHIANG 1992 *Symposium on Flow-Induced Vibration and Noise*, *ASME* **6** (FED/Vol.138/PVP-Vol. 245), 103–112. The study of vortex shedding frequencies behind tapered circular cylinders.
4. D. GERICH and H. ECKELMANN 1982 *Journal of Fluid Mechanics* **122**, 109–121. Influence of end plates and free ends on the shedding frequency of circular cylinders.
5. R. STÄGER and H. ECKELMANN 1991 *Physics of Fluids A* **3**, 2116–2121. The effect of endplates on the shedding frequency of circular cylinders in the irregular range.
6. O. M. GRIFFIN 1985 *Transactions of ASME*: *Journal of Fluids Engineering* **107**, 298–306. Vortex shedding from bluff bodies in shear flow: a review.
7. N. W. M. KO and A. S. K. CHAN 1990 *Experiments in Fluids* **9**, 213–221. In the intermixing region behind circular cylinders with stepwise change of the diameter.

8. R. D. PELTZER and D. M. ROONEY 1985 *Transactions of ASME*: *Journal of Fluids Engineering* **107**, 61–66. Vortex shedding in a linear flow from a vibrating marine cable with attached bluff bodies.
9. B. R. NOACK, F. OHLE and H. ECKELMANN 1991 *Journal of Fluid Mechanics* **227**, 293–308. On cell formation in vortex streets.
10. F. B. HSIAO and C. H. CHIANG 1998 *Experimental Thermal and Fluid Science* **17**, 179–188. Experimental study of cellular shedding vortices behind a tapered circular cylinder.
11. O. M. GRIFFIN and M. S. HALL 1991 *Transactions of ASME*: *Journal of Fluids Engineering* **113**, 526–537. Review—vortex shedding lock-on and flow control in bluff body wakes.
12. C. H. K. WILLIAMSON 1992 *Journal of Fluid Mechanics* **243**, 393–441. The natural and forced formation of spot-like "vortex dislocations" in transition of a wake.
13. F. B. HSIAO and J. Y. SHYU 1991 *Journal of Fluids and Structures* **5**, 427–442. Influence of internal acoustic excitation upon flow passing a circular cylinder.
14. D. JESPERSEN and C. LEVIT 1991 *AIAA 29th Aerospace Sciences Meeting*, Reno, AIAA paper 91-0751. Numerical simulation of flow past a tapered cylinder.
15. P. S. PICCIRILLO and C. W. VAN ATTA 1993 *Journal of Fluid Mechanics* **246**, 163–195. An experimental study of vortex shedding behind linearly tapered cylinders at low Reynolds number.
16. R. C. CHANG, F. B. HSIAO and R. N. SHYU 1992 *Journal of Aircraft* **29**, 823–829. Forcing level effects of internal acoustic excitation on the improvement of airfoil performance.
17. T. WEI and C. R. SMITH 1986 *Journal of Fluid Mechanics* **169**, 513–533. Secondary vortices in the wake of circular cylinders.

APPENDIX A: NOMENCLATURE

D	local diameter of the cylinder
D_1, D_2	diameter at the wide, narrow end of the tapered cylinder
$\bar{D}$	mean diameter of the tapered cylinder ($\bar{D} = (\mathrm{D}_1 + \mathrm{D}_2)/2$)
f_1, f_2, f_3	shedding frequency of the cells from the wide end to the narrow end
f_e, f_r, f_s	excitation, response, vortex-shedding frequency
L	span of the cylinder
$G_{v'}$(f):	energy spectrum of the transverse velocity fluctuations
L_{lock}	spanwise lock-in length
L^+_{lock}, L^-_{lock}	right-hand side, left-hand side, lock-in length between the slot center and the right-hand side, left-hand side, boundary of the lock-in region
L_{slot}	excitation slot length
Re_D, $\mathrm{Re}_{\bar{D}}$	Reynolds number based on the local diameter, the mean diameter
R_f	fineness ratio ($= L/\bar{D}$)
R_T	taper ratio ($= L/(D_1 - D_2)$)
St_D, $\mathrm{St}_{\bar{D}}$	Strouhal number based on the local diameter, the mean diameter
U	free stream velocity
u', u_p	excitation velocity, maximum excitation level, measured at the slot exit in the absence of free stream velocity
X, Y, Z	streamwise, transverse, spanwise co-ordinates
Z_{slot}	location of the slot center